J|A|C|S ARTICLES

Published on Web 12/14/2010

# Gauging the Flexibility of Fluorescent Markers for the Interpretation of Fluorescence Resonance Energy Transfer

Jan J. Rindermann,[†] Yosef Akhtman,[†,‡] James Richardson,[§] Tom Brown,[§] and Pavlos G. Lagoudakis*,[†]

*School of Physics and Astronomy and School of Chemistry, University of Southampton, Highfield, Southampton SO17 1BJ, United Kingdom, and Department of Computer Science, Maths and Physics, The University of the West Indies, Cave Hill, Bridgetown BB11000, Barbados*

Received July 8, 2010; E-mail: pavlos.lagoudakis@soton.ac.uk

***Abstract:*** Intramolecular distances in proteins and other biomolecules can be studied in living cells by means of fluorescence resonance energy transfer (FRET) in steady-state or pulsed-excitation experiments. The major uncertainty originates from the unknown orientation between the optical dipole moments of the fluorescent markers, especially when the molecule undergoes thermal fluctuations in physiological conditions. We introduce a statistical method based on the von Mises−Fisher distribution for the interpretation of fluorescence decay dynamics in donor−acceptor FRET pairs that allows us to retrieve both the orientation and the extent of directional fluctuations of the involved dipole moments. We verify the method by applying it to donor−acceptor pairs controllably attached to DNA helices and find that common assumptions such as complete rotational freedom or fully hindered rotation of the dipoles fail a physical interpretation of the fluorescence decay dynamics. This methodology is applicable in single-molecule and ensemble measurements of FRET to derive more accurate distance estimates from optical experiments, without the need for more complex and expensive NMR studies.

## Introduction

The spectroscopic ruler is a mature tool in the life sciences to probe inter- and intramolecular distances on the nanometer scale by the detection of the distance-dependent fluorescence quenching in a pair of donor−acceptor molecules undergoing fluorescence resonance energy transfer (FRET).[1,2]

The technique can be used in conjunction with microscopy to allow real-time and in vivo observation of the transport, chemical activity, and interactions of proteins and other biomolecules in cells.[3−7] FRET was used to study the DNA holiday junction[8,9] and the kinetics of DNA hairpin loop formation[10] as well as structure/function relationships in a ribozyme[11] and the interaction of the *Escherichia coli* rep helicase with DNA.[12] The use of FRET to study oligonucleotides and the tertiary structure and interactions of RNA has been reviewed.[13,14] The review by Selvin[15] and the references therein discuss the application of FRET to investigate the effect of protein binding on DNA structure. Detailed insight into the stepwise movement of the motor protein Kinesin was gained by labeling its ends with FRET probes.[16,17] Another important application of FRET is monitoring DNA amplification during the polymerase chain reaction.[18] After the observation of FRET between a single donor and single acceptor molecule,[19] the technique is now routinely used at the single-molecule level to study conformational dynamics of proteins and other biomolecules.[20−22] The potential of FRET goes beyond that of a structural tool;

[†] School of Physics and Astronomy, University of Southampton.
[‡] The University of the West Indies.
[§] School of Chemistry, University of Southampton.

(1) Förster, T. *Naturwissenschaften* **1946**, *6*, 166–175.
(2) Stryer, L.; Haugland, R. P. *Proc. Natl. Acad. Sci. U.S.A.* **1967**, *58*, 719–726.
(3) Sekar, R. B.; Periasamy, A. *J. Cell Biol.* **2003**, *160*, 629–633.
(4) Periasamy, A. *J. Biomed. Opt.* **2001**, *6*, 287–291.
(5) Jares-Erijman, E. A.; Jovin, T. M. *Nat. Biotechnol.* **2003**, *21*, 1387–1395.
(6) Galperin, E.; Verkhusha, V. V.; Sorkin, A. *Nat. Methods* **2004**, *1*, 209–217.
(7) Demarco, I. A.; Periasamy, A.; Booker, C. F.; Day, R. N. *Nat. Methods* **2006**, *3*, 519–524.
(8) Miick, S. M.; Fee, R. S.; Millar, D. P.; Chazin, W. J. *Proc. Natl. Acad. Sci. U.S.A.* **1997**, *94*, 9080–9084.
(9) McKinney, S. A.; Déclais, A.-C.; Lilley, D. M. J.; Ha, T. *Nat. Struct. Biol.* **2002**, *10*, 93–97.
(10) Bonnet, G.; Krichevsky, O.; Libchaber, A. *Proc. Natl. Acad. Sci. U.S.A.* **1998**, *95*, 8602–8606.
(11) Zhuang, X.; Kim, H.; Pereira, M. J. B.; Babcock, H. P.; Walter, N. G.; Chu, S. *Science* **2002**, *296*, 1473–1476.
(12) Ha, T.; Rasnik, I.; Cheng, W.; Babcock, H. P.; Gauss, G. H.; Lohman, T. M.; Chu, S. *Nature* **2002**, *419*, 638–641.
(13) Lilley, D. M. J.; Wilson, T. J. *Curr. Opin. Chem. Biol.* **2000**, *4*, 507–517.
(14) Lilley, D. M. J. In *Methods in Enzymology*, Vol. 469; Herschlag, D., Ed.; Elsevier: Amsterdam, 2009; 159−187.
(15) Selvin, P. R. *Nat. Struct. Biol.* **2000**, *7*, 730–734.
(16) Mori, T.; Vale, R. D.; Tomishige, M. *Nature* **2007**, *450*, 750–754.
(17) Verbrugge, S.; Lansky, Z.; Petermann, E. J. G. *Proc. Natl. Acad. Sci. U.S.A.* **2009**, *106*, 17741–17746.
(18) Didenko, V. V. *Biotechniques* **2001**, *31*, 1106–1121.
(19) Ha, T.; Enderle, T.; Ogletree, D. F.; Chemla, D. S.; Selvin, P. R.; Weiss, S. *Proc. Natl. Acad. Sci. U.S.A.* **1996**, *93*, 6264–6268.
(20) Weiss, S. *Nat. Struct. Biol.* **2000**, *7*, 724–729.
(21) Roy, R.; Hohng, S.; Ha, T. *Nat. Methods* **2008**, *5*, 507–516.
(22) Abelson, J.; Blanco, M.; Ditzler, M. A.; Fuller, F.; Aravamudhan, P.; Wood, M.; Villa, T.; Ryan, D. E.; Pleiss, J. A.; Maeder, C.; Guthrie, C.; Walter, N. G. *Nat. Struct. Mol. Biol.* **2010**, *17*, 504–512.

  

ingenious engineered FRET sensors have been used to sense acidity[23] or DNA methylation for cancer cell detection.[24]

The remaining uncertainty in this technique originates from lack of knowledge about the mutual orientation of the dipole moments of the fluorescent markers, a parameter usually expressed through the dimensionless orientation factor $\kappa^2 = [\cos(\Theta_{rel}) - 3\cos(\Theta_D)\cos(\Theta_A)]^2$, where $\Theta_D$ ($\Theta_A$) is the angle between the donor (acceptor) dipole and the axis connecting the dipoles and $\Theta_{rel}$ is the angle between the two dipole moments (Supplementary Figure 4b in the Supporting Information shows the arrangement). Physical rotation and structural conformational fluctuations affect the alignment of the transition moments and necessitate a careful interpretation of the average FRET efficiency obtained in steady-state or time-resolved experiments. Because the rate of FRET scales with $\kappa^2/r^6$, where $r$ is the distance between the donor−acceptor pair, uncertainties in the orientation factor transform into errors in the estimated distance. The twisted DNA helix has proven valuable in detailed studies of the FRET process, as it allows control of both the separation distance and orientation between a donor−acceptor pair of fluorescent markers.[25,30] Recent studies revealed that neither a rigid dipole behavior nor the assumption of fast and isotropic rotation ($\kappa^2 = 2/3$) complies with the experimental observation of a periodic modulation of the FRET efficiency as the donor−acceptor separation increases along the twisted helix.[26−28] Although restriction of rotational motion of the fluorescent dyes is evident in these experiments ($\kappa^2 \neq 2/3$), its quantitative description is not fully explored.[27,29,30] In this work we combine experiment- and simulation-based methodology to retrieve the mean direction, orientational spread, and corresponding orientation factors of the fluctuating donor and acceptor transition dipoles of a typical FRET pair from the characteristic dynamics of the fluorescent decay curves, a feature often overlooked in quantitative analyses. This information can be used directly to increase the precision of quantitative FRET experiments. We demonstrate and verify the procedure on a series of donor−acceptor (Fluorescein dT−Texas red) FRET pairs controllably attached to double-stranded DNA via six-carbon linkers. Thermal fluctuations of the dipoles around their equilibrium orientation are incorporated into the simulation of FRET using the von Mises−Fisher distribution, a physical, unimodal distribution function for vectors. The simulation yields measurable quantities like the average FRET efficiency and the fluorescence decay curve of the donor, which are compared with their experimental counterparts.

## Results

**Fluorescence Decay Curves Reveal Fluctuating Dipole Orientation.** We apply spectrally filtered time-correlated single-photon counting (TCSPC) under nonresonant excitation to measure the fluorescence decay curves of the donors in ensembles of FRET pairs where $n$, the number of bases along the helix separating the dye molecules, takes the following values: $n = 5$, 7, 10, 12, 13, 15, 17, 20, and 22. These are depicted in Figure 1d (green curves), along with the chemical structure of the dyes (Figure 1a,b) and a schematic of a double-labeled DNA molecule (Figure 1c). The graph for $n = 5$ additionally shows the fluorescence decay of a control sample labeled with the donor (Fluorescein dT) only (gray curve). Evidently, the fluorescence is quenched in the presence of the acceptor on the DNA molecule, and the curves for small $n$ show a clear deviation from an exponential decay law, reproducing the observations from refs 27 and 28. Fitting such decay dynamics with a multiexponential function presumes different subensembles of excited donor molecules with different recombination decay rates, which we have ensured is not the case in our study. (See the chemical structure of the dyes (Figure 1a,b) and Supporting Information, Sample preparation, Supplementary Figure 1, and Supplementary Tables 1 and 2, for details on the chemical synthesis.) The negatively charged dyes are repelled by the DNA backbone and cannot attach to the DNA in

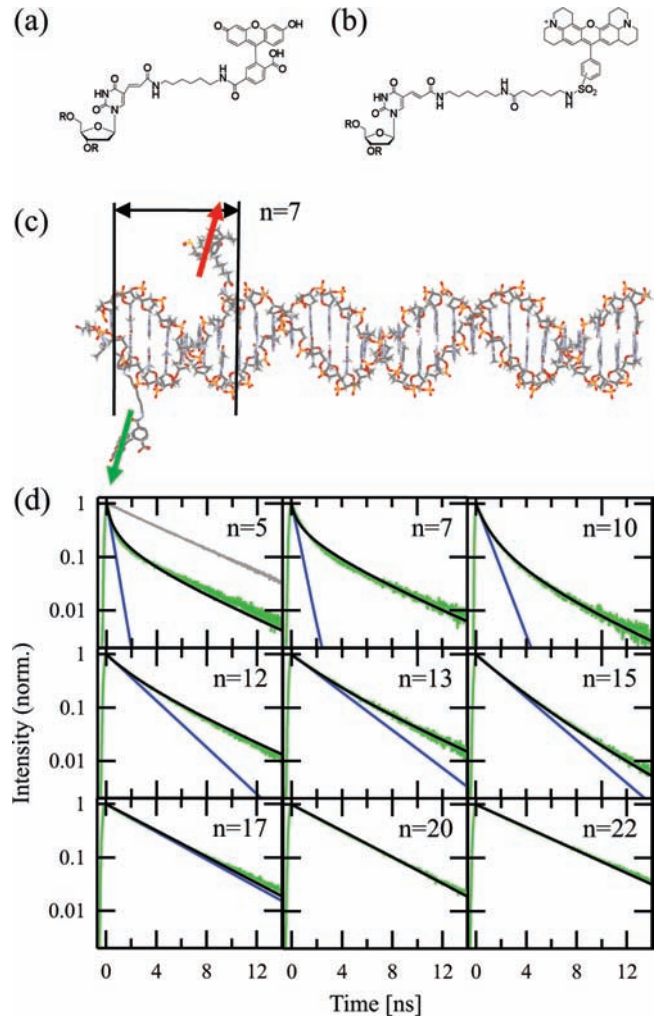


***Figure 1.*** FRET between a donor−acceptor pair in a controlled geometry. (a,b) Chemical structure of Fluorescein dT and Texas red-labeled aminoC6dT as present in the labeled oligonucleotides. (c) Double-labeled DNA helix with $n = 7$. (d) Fluorescence decay curves of the donor (green curves) in ensembles with different separation number $n$. Black curves, simulated decay from the best-fit parameters; blue curves, simulated decay from the best-fit parameters in the dynamic averaging regime; gray curve, decay of the donor in the absence of a FRET acceptor.

(23) Modi, S.; Swetha, M. G.; Goswami, D.; Gupta, G. D.; Mayor, S.; Krishnan, Y. *Nature Nanotechnol.* **2009**, *4*, 325–330.
(24) Feng, F.; Liu, L.; Wang, S. *Nature Protoc.* **2010**, *5*, 1255–1264.
(25) Clegg, R. M.; Murchie, A. I. H.; Zechel, A.; Lilley, D. M. J. *Proc. Natl. Acad. Sci. U.S.A.* **1993**, *90*, 2994–2998.
(26) Lewis, F. D.; Zhang, L.; Zuo, X. *J. Am. Chem. Soc.* **2005**, *127*, 10002–10003.
(27) Iqbal, A.; Arslan, S.; Okumus, B.; Wilson, T. J.; Giraud, G.; Norman, D. G.; Ha, T.; Lilley, D. M. J. *Proc. Natl. Acad. Sci. U.S.A.* **2008**, *105*, 11176–11181.
(28) Börjesson, K.; Preus, S.; El-Sagheer, A. H.; Brown, T.; Albinsson, B.; Wilhelmsson, L. M. *J. Am. Chem. Soc.* **2009**, *131*, 4288–4293.
(29) Xu, Q.-H.; Wang, S.; Korystov, D.; Mikhailovsky, A.; Bazan, G. C.; Moses, D.; Heeger, A. J. *Proc. Natl. Acad. Sci. U.S.A.* **2005**, *102*, 520–535.
(30) Hochstrasser, R. A.; Chen, S.-M.; Millar, D. P. *Biophys. Chem.* **1992**, *45*, 133–141.

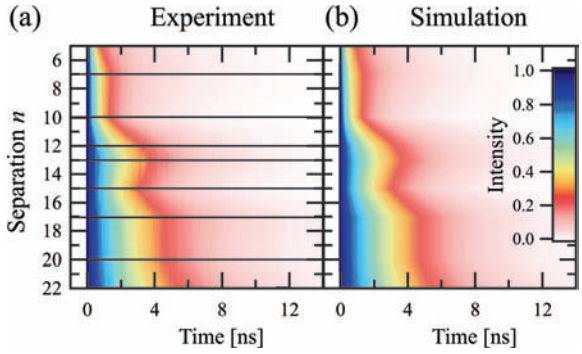


***Figure 2.*** False color representation of fluorescence decay curves of donors in ensembles with different separation number *n*. (a,b) Linearly interpolated experimental and numerical decay curves. The black lines indicate the decays shown in Figure 1d.

conformations that would result in different dipole orientations and decay dynamics. Therefore, we consider the nonexponential fluorescence decay dynamics as a genuine feature of the FRET process. Another feature becomes apparent in Figure 2a: Here the different decay curves are plotted in a false color image, where the intensity at a certain time and separation number *n* is represented with a color. The black lines in Figure 2a correspond to the fluorescence decay curves shown in Figure 1d. The two-dimensional image is produced using linear interpolation between the experimental values of *n* to reveal the following trend: fast and slow decays alternate as *n* increases. This is due to the helical twist of the DNA, which results in alternating parallel and orthogonal dipole orientations for increasing *n*. In general, the helical twist also causes a modulation of the distance between the dyes, which in the case of sufficiently short linker molecules is monotonous and does lead to an oscillatory behavior. We chose the separation number *n* of the samples deliberately to resolve this alternation, which occurs with a period of 2−3 base pairs. It gives rise to the oscillation of the FRET efficiency with increasing *n*, which can be independently measured in steady-state experiments and will be discussed separately.

From the described features of the fluorescent decay curves of the donors, two conclusions can be derived: First, the dipole moments of the acceptor and donor molecules do not randomize over all orientations on a shorter time scale compared to the reciprocal FRET rate. If this were the case, fast and slow decays would not alternate due to the twist of the helix, as complete rotational freedom yields the same average orientation factor for all separation distances. Second, the dipole moments must experience some degree of rotational freedom, as we do not observe a nearly complete suppression of FRET for values of *n* between 5, 10, 15, and 20, where we would expect approximately orthogonal orientation between the electric field of one dipole and the dipole moment of the other at one particular separation distance. This leads to the interpretation of the nonexponential decay curves as a superposition of decays from donor−acceptor pairs with varying orientation factors. An additional distribution of different donor−acceptor distances cannot be ruled out, but this can be seen as a higher order correction since inclusion of a distribution of distances for otherwise identically oriented dipoles cannot explain a nonzero FRET efficiency for mutual orthogonal orientation. In contrast, a distribution of slightly differently aligned dipoles separated by a constant distance yields a distribution of FRET efficiencies which are larger than zero, even if the dipoles are oriented orthogonally on average. Therefore, we model the FRET process in a first approximation by accounting for fluctuations in the dipole orientations only.

**Dipole Reorientation Rate.** In the case of dipoles which do not reorient on the time scale of the reciprocal rate of FRET (static average regime), the decay dynamics and the average FRET efficiency in the ensemble are determined by a continuous superposition of FRET rates for differently oriented dipoles. If the rotational correlation time of the dipoles is short compared to the reciprocal FRET rate, the decay dynamics and the FRET efficiency are characterized by dynamically averaged values. We measure the time-resolved fluorescence anisotropy from samples labeled with Fluorescein dT or Texas red only to estimate the rotational correlation times of the dye molecules attached to the much larger DNA molecule. The rotational correlation times are 0.50 ns for Fluorescein dT and 1.31 ns for Texas red. (See Supporting Information, Time-resolved anisotropy, Supplementary Table 3, and Supplementary Figures 2 and 3 for the setup and results of the anisotropy measurements.) The reciprocal rotational correlation times will have to be compared with the FRET rate in order to implement the static or dynamic averaging regime in the FRET simulation.

**Quantifying the Dipoles' Fluctuations with the von Mises−Fisher Distribution.** Following the temporal characterization of the dyes' rotational motion, the extent of these random fluctuations is accounted for in the modeling of the FRET process. Without loss of generality, full and partial rotational freedom of the dipole vectors can be described with a unimodal probability density function for the dipole vector orientation. Here we choose the von Mises−Fisher distribution, the analogue of the Gaussian distribution for the analysis of directional data in three dimensions.[31] Relative to a mean direction defining the $z'$-axis of a frame of reference $S'$, the normalized von Mises−Fisher distribution is given by

$$F(\theta', \phi') = \frac{c}{4\pi \sinh(c)} \exp(c \cos(\theta')) \qquad (1)$$

where $\theta'$ is the polar angle measured from the mean direction, $\phi'$ is the azimuth measured from an arbitrarily chosen $x'$-axis perpendicular to the mean, and $c = 1/\sigma^2$ is a concentration factor which determines the width $\sigma$ of the cylindrically symmetric distribution. Figure 3a depicts three such von Mises−Fisher distributions of different widths. In the case of slow reorientation of the dipoles compared to the reciprocal energy-transfer rate, the probabilistic knowledge of the orientation factor in one donor−acceptor pair can be transferred to the relative frequency of the corresponding energy-transfer rate in a large ensemble of identical pairs. Additionally, during the optical measurements, the molecules assume all possible conformations due to thermal fluctuations.

**Modeling FRET between Two Fluctuating Dipoles on Helical DNA.** Modeling of the FRET process requires a geometric parametrization of the position and orientation of the donor and acceptor dipole moments on the DNA strand. Independent of the separation number *n*, the dye positions relative to the DNA are described using the geometric parameters introduced by Clegg:[25] $r_l$ is the deflection of the dyes from the center of the helix due to the linker molecules, and $L$ and $\phi_{rel}$ are the offsets in the position of the dyes along the helix and in the radial orientation of the linker molecules for the donor and acceptor if they were attached to the same base. (Supple-

(31) Fisher, R. *Proc. R. Soc. London, Ser. A* **1953**, *217*, 295–305.

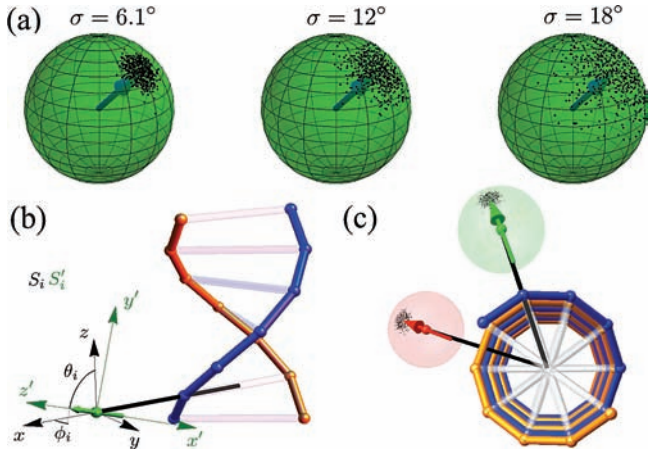


***Figure 3.*** Definition of geometric parameters in the model. (a) Random fluctuations of a vector's orientation according to the von Mises−Fisher distribution. The distribution is shown for different widths. (b) Relation between the $S_i$ and $S'_i$ coordinate systems. $\theta_i$ and $\phi_i$ define the average orientation of the dipole relative to the DNA strand. (c) View from the top on the donor−acceptor-labeled DNA helix with $n = 7$. The green (red) solid spheres and arrows represent the position and orientation of the optical dipole of the donor (acceptor).

mentary Figure 4 in the Supporting Information shows $r_l$, $L$, and $\phi_{rel}$ in detail.) In the dye−linker systems used here, the dyes, Fluorescein dT and Texas red, are negatively charged and the linkers are hydrophobic. Given the negatively charged, hydrophilic DNA backbone, we assume the dye−linker equilibrium position to be almost perpendicular to the DNA central axis, as shown in Figure 1c. The average orientation of the donor (D) and acceptor (A) dipole is described in spherical coordinates $(\theta_D,\phi_D)$ and $(\theta_A,\phi_A)$ in the coordinate systems $S_D$ and $S_A$, respectively. These reference systems share a common $z$-axis ($\theta_{i=D,A} = 0$) directed along the long axis of the DNA helix, whereas the $x_i$-axes, where $\phi_i = 0$, are defined by the respective linker molecule (see Figure 3b and Supplementary Figure 4a). For any static pair of donor−acceptor dipoles, the energy-transfer rate is calculated from their mutual orientation and separation distance according to the Förster theory,[1] taking into account the configuration of the DNA and the linker molecules.

In the static averaging regime, the fluorescence decay of the donors undergoing energy transfer is a superposition of contributions from many differently oriented dipole pairs, each occurring with a probability according to the von Mises−Fisher distributions of the donor and acceptor. The fluorescence decay after a short excitation pulse is then given by[32]

$$\langle I(t)\rangle_{st} \propto \int\int F_D(\theta'_D,\phi'_D)\, F_A(\theta'_A,\phi'_A)\, e^{-(k_{D,rad}+k_{FRET}(\theta'_D,\phi'_D,\theta'_A,\phi'_A))t}\, d\Omega'_D\, d\Omega'_A \quad (2)$$

where $k_{FRET}$ is the energy-transfer rate, $k_{D,rad}$ is the radiative decay rate of the donor molecule, and $d\Omega'_i = \sin\theta'_i\, d\theta'_i\, d\phi'_i$ is the element of solid angle in the $S'_{i=D,A}$ coordinate system depicted in Figure 3b. In the presence of nonradiative decay mechanisms other than FRET, their respective rates are added to the sum in the exponent. The integration is performed over all possible orientations. The energy-transfer rate $k_{FRET}$ depends strongly on the angular variables $\theta'_D$, $\phi'_D$, $\theta'_A$, $\phi'_A$ through the orientation factor $\kappa^2$, and evaluation of $\kappa^2$ requires the transformation of the coordinates used in eq 2 to a common reference system (see Supporting Information, Coordinate transformations). In general, the above expression results in nonexponential decay dynamics which are more pronounced when the distance is small and $k_{FRET}$ is large. The average FRET efficiency $\langle\eta_{FRET}\rangle_{st}$ and average orientation factor $\langle\kappa^2\rangle_{st}$ in the static averaging regime can be calculated in analogy to the ensemble fluorescence intensity in eq 2 by replacing the exponential factor with the efficiency $\eta_{FRET} = k_{FRET}/(k_{D,rad} + k_{FRET})$ or $\kappa^2$ of an individual dipole pair. Here, all other competing nonradiative recombination mechanisms are neglected (donor quantum yield of 100%).

Calculation of the *dynamically* averaged orientation factor for fast-fluctuating dipoles with a given distribution function follows the formalism introduced by Dale and Eisinger[33] and van der Meer,[34,35] which we adapt to the von Mises−Fisher distribution. The depolarization factors $d_D$ and $d_A$ for the donor and acceptor dipole and the dynamically averaged orientation factor $\langle\kappa^2\rangle_{dyn}$ are estimated according to ref 35. (See Supporting Information, Dynamic averaging regime, for the calculation.) The dynamically averaged FRET efficiency $\langle\eta_{FRET}\rangle_{dyn}$ can be calculated from the corresponding rate $\langle k_{FRET}\rangle_{dyn}$, which is obtained by setting $\kappa^2 = \langle\kappa^2\rangle_{dyn}$ in the expression for the energy-transfer rate.[1] This results in an exponential fluorescence decay of the form

$$\langle I(t)\rangle_{dyn} \propto e^{-(k_{D,rad}+\langle k_{FRET}\rangle_{dyn})t} \quad (3)$$

See the Methods section for the determination of the constants in the above expressions.

**Simultaneous Analysis of the Fluorescence Decay Curves.** The fluorescent decay curves are quantitatively analyzed with eqs 2 and 3. A global fitting procedure analyzes all decay curves simultaneously with the same set of geometric parameters. This is required because, even for decay curves with pronounced nonexponential decay dynamics, the best-fit parameters resulting from a singular fit are not unique and depend on the initial values of the fitting parameters and numerical inaccuracies. The fitting parameters are the mean orientation of the donor and acceptor dipole moments relative to the DNA, the width of their fluctuations, and the Clegg parameters $r_l$, $L$, and $\phi_{rel}$. Because the linker molecules of the donor and acceptor molecule are the same, the radial displacement $r_l$ of the dyes from the center of the DNA and the width of the dipole fluctuations are assumed to be equal for both dyes. This reduces the number of independent parameters in the fitting procedure. The fitting parameters are assumed to be equal for all samples, except that the sign of the offsets $L$ and $\phi_{rel}$ depends on the order of the dyes along the labeled sequence. Sequence-dependent conformational changes are neglected here, as the neighboring bases to the linker molecules are virtually the same for both Fluorescein dT and Texas red (see Supplementary Table 1). If the samples, which differ only with respect to the separation number $n$ and the order of donor and acceptor along the helix, did not have this similarity, it would not be possible to exploit the strong constraints the global analysis puts onto the fitting parameters.

Lack of a priori knowledge of the separation number $n$ at which the reciprocal rotational correlation time starts to exceed

(32) Wu, P.; Brand, L. *Biochemistry* **1992**, *31*, 7939–7947.
(33) Dale, R. E.; Eisinger, J.; Blumberg, W. E. *Biophys. J.* **1979**, *26*, 161–194.
(34) van der Meer, B. W.; Raymer, M. A.; Wagoner, S. L.; Hackney, R. L.; Meechem, J. M.; Gratton, E. *Biophys. J.* **1993**, *64*, 1243–1263.
(35) van der Meer, B. W. *Mol. Biotechnol.* **2002**, *82*, 181–196.

***Table 1.*** Geometric Parameters Obtained from the Simultaneous Fitting Procedure

| | | | |
|---|---|---|---|
| $\phi_D$ | 2.3° | $\sigma$ | 6.1° |
| $\theta_D$ | 126° | $r_l$ | 1.33 nm |
| $\phi_A$ | −3° | $L$ | 0.14 nm |
| $\theta_A$ | 134.2° | $\phi_{rel}$ | −54° |

the FRET rate and the dynamic averaging regime applies necessitates a recursive procedure for fitting the decay curves. At first we apply an intermediate simultaneous fit to all decay curves, assuming that all samples fall within the static averaging regime. The best-fit parameters are used in a Monte Carlo simulation for different values of $n$ that simulates large ensembles ($N = 5 \times 10^5$) of FRET pairs where the individual donor and acceptor dipoles are distributed randomly around their average orientations according to the given von Mises−Fisher distributions. In contrast to the direct numerical evaluation of eq 2, this approach gives histograms of the occurrence of certain values for $\kappa^2$, $k_{FRET}$, and $k_{FRET,max}$, the maximum rate of FRET in the ensemble, for each $n$. We compare the reciprocal rotational correlation times of Fluorescein dT and Texas red with $k_{FRET,max}$ for different $n$ and find that, for $n > 17$, the value of $k_{FRET,max}$ becomes lower than both reciprocal rotational correlation times, suggestive of the dynamic averaging regime for these $n$. This additional knowledge is applied in the final simultaneous fit of all fluorescence decay curves where, for $n > 17$, the dynamic averaging regime is used. The final parameters yield a smaller $\chi^2$ and differ by less than 2% from the intermediate results. The best-fit curves are plotted in Figure 1d as black lines on top of the experimental data (green). Evidently, the simulation reproduces the nonexponential decay curves based on the implementation of fluctuations in the three-dimensional dipole orientations. For the samples where the static averaging regime applies, the fluorescence decay is also simulated in the dynamic averaging regime using the same parameters (blue curves in Figure 1d). For small distances, when orientational fluctuations lead to very different FRET rates, the dynamic regime overestimates the rate of FRET. With the parameters from the best fit, we produce a false color image representing the fluorescence decay curves for different values of $n$. This is shown in Figure 2b in comparison with the experimental data (Figure 2a). For intermediate values of $n$, the image is linearly interpolated. The numerical results show the same features as the experimental data: alternating fast and slow decays as expected from the twist of the DNA helix. From the fitting procedure, the distance between the electronic dipoles in the dye molecules and the center of the helix is determined as 1.33 nm, which accurately reflects the chemical structure of the six-carbon linker molecules. The orientation and distribution of the transition dipoles for a molecule with $n = 7$ is shown in Figure 3c. Table 1 lists the best-fit parameters, and the left sphere in Figure 3a shows a directional spread of the corresponding width.

**Estimation of the Uniqueness of the Best Fit.** Considering the high dimensionality of the parameter space in the fitting procedure and the complex structure of the $\chi^2$-field, it is necessary to gain confidence in the uniqueness of the best-fit parameters before they can be interpreted any further. Each parameter has a distinct geometric meaning, and none of them is a general amplitude factor which scales the FRET rate arbitrarily to match the simulated with the experimental data. All scaling factors and material constants influencing FRET were determined experimentally (see Methods section) or taken from the literature. Whereas the parameters $r_l$ and $L$ approach their

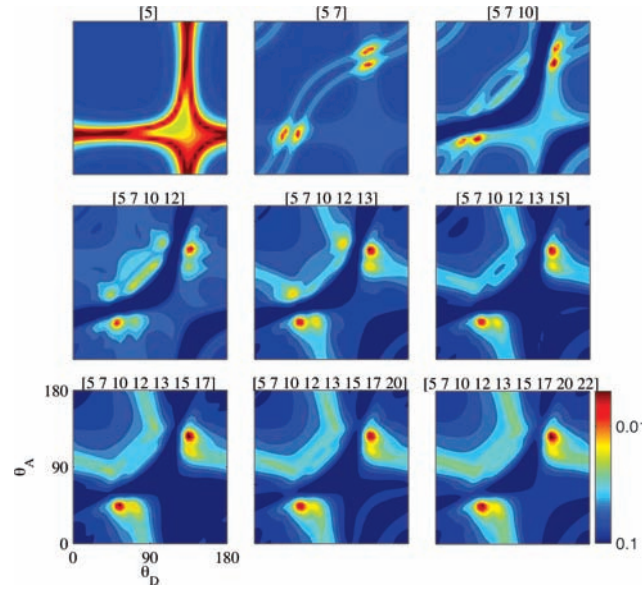


***Figure 4.*** Calculated $\chi^2$ for variations of $\theta_D$ and $\theta_A$ around best-fit values. All other parameters are held constant. The numbers above each picture indicate which decay curves were considered for the calculation of $\chi^2$. When more decay curves are included in the analysis, the range of values for $\theta_D$ and $\theta_A$ that yield an equally good fit reduces to a single point in parameter space (see text for discussion of the symmetry). The angles are measured in degrees.

single optimum value during the global fit given any other values for the remaining parameters, the angular variables and $\sigma$ only collectively converge to their optimum values, underlining the strong effect of the orientation factor on FRET. The uniqueness of the best-fit parameters is estimated by varying pairs of parameters over a wide range while holding the others constant at their value from the best fit and calculating the resulting $\chi^2$. Figure 4 shows how $\chi^2$ changes when the two polar angles $\theta_D$ and $\theta_A$ of the mean donor and acceptor dipole orientation are varied. $\chi^2$ is calculated for different cases where not all but an increasing number of decay curves are considered simultaneously. Starting from the first decay ($n = 5$), more curves are subsequently included in the determination of $\chi^2$ to show the increasing constraints on the parameters imposed by the global fit. In fact, if only one curve is fitted, bands of equal $\chi^2$ can be found in the exemplary two-dimensional parameter scans shown in Figure 4, whereas only a small region with a unique pair of parameters evolves as the number of simultaneously considered curves increases. When more decay curves are included in the global fit, the system becomes strongly constrained, as each curve's individual shape imposes a strong restraint. The constraint is stronger than that of a single point which would be used, for instance, if the experimental FRET efficiency vs $n$ curve were subject to a fitting procedure. From symmetry arguments one would expect the same FRET dynamics from all samples under a mirror symmetry transformation of the polar angles [$\theta_D = 180° - \theta_A$, $\theta_A = 180° - \theta_D$], which satisfactorily appears in the $\chi^2$ plots of Figure 4. This shows that, within the framework of the developed model, only the presented best-fit parameters reproduce well the peculiar fluorescence decay dynamics of the samples. These tests are also performed pairwise for the parameters ($\phi_D$, $\phi_A$) and ($L$, $\phi_{rel}$) with similar results (see Supporting Information, Supplementary Figure 5).

**Comparison of Time-Resolved and Time-Integrated Results.** The effect of the helical twist on the distribution of the orientation factor in the ensemble can be understood

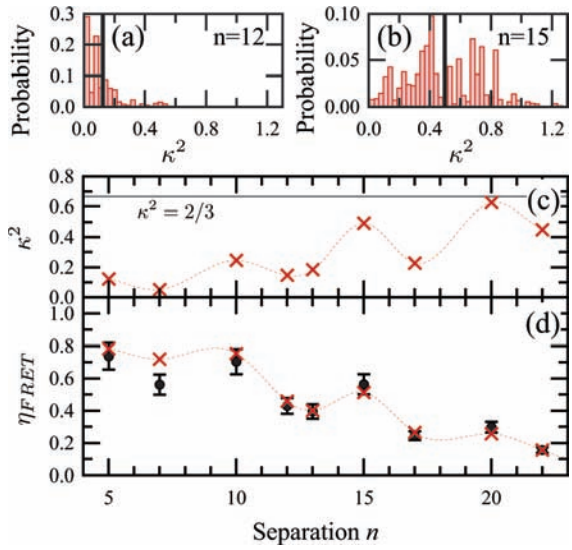


***Figure 5.*** Orientation factor $\kappa^2$ and FRET efficiency $\eta_{FRET}$ in ensembles with different separation number $n$. (a,b) Probability distribution of the orientation factor for $n = 12$ and $n = 15$. The black bars indicate the centers of mass of the distributions. (c) Average orientation factor (dotted line is a guide to the eye). (d) FRET efficiency. The red crosses are the calculated ensemble averages (dotted line is a guide to the eye), and the black dots are the steady-state results. The error bars are calculated from the experimental accuracy of the concentration of the solutions.

quantitatively from two typical histograms of the orientation factor for $n = 12$ and $n = 15$ showed in Figure 5a,b. The histograms are produced using the parameters of the best global fit. (See Supporting Information, Supplementary Figure 6, for all computed histograms.) Clearly the distribution for $n = 15$ incorporates larger values of the orientation factor than the one for $n = 12$, and besides the fluctuations intrinsic to the Monte Carlo approach, the distributions exhibit a nontrivial shape around their centers of mass. For $n = 15$, the mean (0.45) is near the often assumed value for the orientation factor of $\kappa^2 = 2/3$, whereas for $n = 12$ it lies well below (0.14). Similar observations have been made by Dolghih et al., who found that even two distributions with similar mean values lead to noticeably different average FRET efficiencies in the ensemble.[36] Although the distance between the dyes is longer for $n = 15$ than for $n = 12$, energy transfer is more favorable for $n = 15$ due to the frequent occurrence of larger orientation factors. Figure 5c shows the average orientation factor of the ensemble (red crosses) exhibiting an oscillatory behavior with a period of 5 bp. These oscillations can be found again in the dependency of the FRET efficiency on the separation number $n$ as measured from the enhanced steady-state fluorescence of the acceptor (black dots) shown in Figure 5d. The simulated FRET efficiency of the ensemble (red crosses) is in good agreement with the steady-state results. In agreement with previous reports, the FRET efficiency does not reach values close to zero at separations $n$ for which one would expect perpendicular orientation between the electric field of one dipole and the dipole moment of the other, indicative of a distribution of orientation factors in the ensemble.[27,28]

## Discussion

In conclusion, we present a statistical method to retrieve information about the orientational freedom of dye−linker complexes from the characteristic shape of the fluorescence decay curves of FRET pairs, a necessity to overcome uncertainties in distance determination due to the unknown orientation factor. The ensemble fluorescence results from the static or dynamic average of contributions from individual donor−acceptor pairs with fluctuating dipole moments. For the first time, multiple fluorescence decay curves from different donor−acceptor-labeled DNA helices are analyzed simultaneously and with a fluorescence decay model that accounts for the observed nontrivial decay dynamics. As a result of the orientational freedom of the dye molecules, a nonzero FRET efficiency is measured and calculated for ensembles where the average dipole orientation is nearly orthogonal, omitting FRET in the rigid dipole approximation. From the simulation it can be seen that the nontrivial distribution of the orientation factor $\kappa^2$ oscillates depending on the separation between the dyes along the DNA helix and cannot be characterized for all samples with a mean value of $\kappa^2 = 2/3$, which would correspond to complete rotational freedom. The output parameters of the presented analysis are the relative position, the average orientation of the optical dipoles relative to the DNA, and the magnitude of their orientational fluctuations. The models output can be further improved by restraining some of the fitting parameters with additional information about the molecular conformation of the samples from molecular dynamics simulations or NMR experiments. The presented methodology has relevance for all FRET experiments in which partial rotational freedom of the fluorescent markers is expected and could be further quantified in order to separate uncertainties in the orientation factor from those in the determined distance.

## Materials and Methods

**Time-Resolved Fluorescence Decay Measurements Using TCSPC.** The fluorescence decay curves were measured by time-correlated single photon counting (TCSPC) with a fast data acquisition card and a frequency-doubled ultrafast laser, giving 180 fs pulses at 400 nm at a repetition rate of 250 kHz, in conjunction with a monochromator and an avalanche photodiode. The monochromator was set to a spectral window of ±5 nm at the donor emission wavelength at 525 nm. The excitation power of 1.5 mW was chosen low enough to avoid photobleaching of the fluorescent dyes over the time span of the experiment. The fluorescence decays were measured on a time range of 43 ns resolved into 4096 channels, with resolution of 230 ps (fwhm).

**Time-Resolved Fluorescence Anisotropy Measurements Using a Streak Camera.** Samples labeled with donor or acceptor only were excited with a vertically polarized laser (400 nm, 180 fs pulses, 250 kHz repetition rate), and the fluorescence was collected at an angle of 90° to the excitation beam before it was sent through a Wollaston prism to separate the propagation direction of vertically and horizontally polarized light by 5°. The fluorescence was then focused into a streak camera, where the time dynamics of both polarizations could be measured simultaneously, circumventing uncertainties related to photobleaching or fluctuating excitation power during the experiment. (See Supplementary Figure 2 for the setup.)

**Experimental Constants.** For the evaluation of eqs 2 and 3, the following constants are used: The fluorescence decay rate of the donor in the absence of FRET is determined from a control sample of b-DNA labeled with the donor only as $k_{D,rad} = 0.208455$ ns$^{-1}$, where the high quantum yield of Fluorescein dT, $Q_D = 0.96$, allows us to neglect any other nonradiative recombination mechanisms in the calculations. The refractive index for the aqueous solutions is set to $n = 1.33$. The donor−acceptor spectral overlap was calculated from the emission of a sample labeled with Fluorescein dT (donor) only and the absorbance from a sample

(36) Dolghih, E.; Roitberg, A. E.; Krause, J. L. *J. Photochem. Photobiol. A: Chem.* **2007**, *190*, 321–327.

labeled with Texas red (acceptor) only. For comparison, the Förster radius for this FRET pair is calculated to be 5.8 nm, based on the assumption of $\kappa^2 = 2/3$. We assume the standard geometry of b-DNA with 10.5 bp per turn and a helical rise of 0.33 nm.

**Computational Methods.** The simultaneous fitting of the fluorescence decay curves was performed using a self-written program in C++ running on a multicore computer at the School of Engineering and Computer Science, University of Southampton. High computing power is essential to evaluate the four-dimensional integrals hundreds of times during the fitting procedure. The procedure minimizes $\chi^2$, the sum of the weighted squared differences between the simulated and experiment data, deploying the Levenberg−Marquardt algorithm. The complexity of the $\chi^2$-field required manual and random checks on the dependence of the result on the initial values of the parameters to ensure a unique set of parameters was found. The weighting factor is the standard deviation of the experimental data and is estimated from the Poisson noise in the photon counting ($\sqrt{I(t)}$). The integrals are solved by trapezoidal integration. The decay curves needed to be sampled at 201 points for 15 ns of the decay instead of the initial 4096 for 42 ns in order to achieve reasonable computation time. It was ensured that the result of the fitting procedure does not depend on the sampling rate or the initial values of the parameters. The histograms for the orientation factor in the different ensembles were obtained by a Monte Carlo simulation using Igor Pro, Wavemetrics. The accuracy of both methods was adjusted such that the error in the numerical integration was less than 4%.

**Acknowledgment.** J.J.R. appreciates funding from the Reiner-Lemoine-Stiftung, Germany. This research has received funding from the European Community's Seventh Framework Programme [FP7/2007−2013] under agreement numbers 248855 entitled "Nanophotonics for energy efficiency", 237900 entitled "ICARUS", and HEALTH-F4-2008-201418 entitled "READNA", and from the EPSRC through EP/F013876/1 and EP/G063494/1.

**Supporting Information Available:** Sample preparation; details on the measurement of time-resolved anisotropy, coordinate transformations in the simulation, and the dynamic averaging regime. This material is available free of charge via the Internet at http://pubs.acs.org.

JA105720J